JBC RESEARCH ARTICLE

Structural basis for juvenile hormone biosynthesis by the juvenile hormone acid methyltransferase

Received for publication, August 9, 2021, and in revised form, September 19, 2021 Published, Papers in Press, September 23, 2021,
https://doi.org/10.1016/j.jbc.2021.101234

Pengchao Guo[1,2,‡], **Yunshi Zhang**[1,2,‡], **Li Zhang**[1,2,‡], **Haiyang Xu**[1,2], **Huan Zhang**[1,2], **Zhan Wang**[1,2], **Yongliang Jiang**[3], **David Molloy**[4], **Ping Zhao**[1,2,*], **and Qingyou Xia**[1,2,*]

From the [1]*State Key Laboratory of Silkworm Genome Biology, Biological Science Research Center and* [2]*Chongqing Key Laboratory of Sericultural Science, Chongqing Engineering and Technology Research Center for Novel Silk Materials, Southwest University, Chongqing, China;* [3]*Hefei National Laboratory for Physical Sciences at the Microscale and School of Life Sciences, University of Science and Technology of China, Hefei, Anhui, China;* [4]*School of Basic Medical Science, Chongqing Medical University, Chongqing, China*

Edited by Joseph Jez

Juvenile hormone (JH) acid methyltransferase (JHAMT) is a rate-limiting enzyme that converts JH acids or inactive precursors of JHs to active JHs at the final step of JH biosynthesis in insects and thus presents an excellent target for the development of insect growth regulators or insecticides. However, the three-dimensional properties and catalytic mechanism of this enzyme are not known. Herein, we report the crystal structure of the JHAMT apoenzyme, the three-dimensional holoprotein in binary complex with its cofactor S-adenosyl-L-homocysteine, and the ternary complex with S-adenosyl-L-homocysteine and its substrate methyl farnesoate. These structures reveal the ultrafine definition of the binding patterns for JHAMT with its substrate/cofactor. Comparative structural analyses led to novel findings concerning the structural specificity of the progressive conformational changes required for binding interactions that are induced in the presence of cofactor and substrate. Importantly, structural and biochemical analyses enabled identification of one strictly conserved catalytic Gln/His pair within JHAMTs required for catalysis and further provide a molecular basis for substrate recognition and the catalytic mechanism of JHAMTs. These findings lay the foundation for the mechanistic understanding of JH biosynthesis by JHAMTs and provide a rational framework for the discovery and development of specific JHAMT inhibitors as insect growth regulators or insecticides.

Juvenile hormones (JHs) are critical for the regulation of a variety of physiological processes in insect development, metamorphosis, and reproduction (1, 2). JHs are lipophilic sesquiterpenoid molecules synthesized by and secreted from the corpora allata (CA), a pair of endocrine glands of the maxillary segment with nerve connections to the brain (3, 4). Eight forms of the secreted hormone have been characterized that differ in side-chain length or epoxidation status. Among this class of hormones, JH III is the simplest and most widespread within insects. JH 0, I, II, and 4-methyl JH I appear to be almost exclusively within *Lepidoptera* spp. (5–7), while a bis-epoxide form, JH III (JHB_3), and its precursor methyl farnesoate (MF) are deemed of prevalence within *Drosophila melanogaster* (8, 9) and *Crustacea* spp. (10). Interestingly, a separate bis-epoxide analogue of JH III ($JHSB_3$) has been identified as the active JH in predacious *Heteropteran* insects (11).

In general, the levels of JH are strictly controlled through reciprocal *de novo* biosynthetic and JH-degradation pathways, with the former considered to overarch JH levels (4, 12). The biosynthesis of JHs involves a bipartite pathway, with an early mevalonate synthesis step and a subsequent JH-branch step (13). The early stage is required for the formation of the farnesyl pyrophosphate (FPP), a central hub substrate in the biosynthesis of cholesterol and other bioactive terpenoids in most living organisms (14). The JH-branch step, in which FPP is converted to active JHs by several enzymes, is unique to insects (15, 16). In this step, S-adenosyl-L-methionine (SAM)-dependent JH acid methyltransferase (JHAMT) is required for catalysis in the final reaction in which the carboxyl group of JHI, II, III acids (JHAs) and farnesoic acid (FA) are methylated generating the corresponding active JH compounds (16, 17). In this catalysis, the SAM molecule is an essential cofactor that provides the methyl group to a substrate and generates the corresponding product S-adenosyl-L-homocysteine (SAH) (18).

The gene encoding JHAMT was first characterized from *Bombyx mori* as a recombinant isoform that was demonstrated to possess methyltransferase activity in the presence of both JHAs and FA substrates (16). Subsequently, orthologues were identified across other insect species (19–21) in which *JHAMT* transcripts were detected to be almost exclusively within the CA tissue. Interestingly, the developmental expression profiles of these insects showed a high correlation to changes in JH titer. Furthermore, transcription activator-like effector nucleases-mediated *JHAMT* knockout in *B. mori* resulted in the death of half the hatched larvae numbers at the first or second larval instar, with survivors undergoing precocious metamorphosis after the third instar (22). Furthermore,

‡ These authors contributed equally to this work.
* For correspondence: Qingyou Xia, xiaqy@swu.edu.cn; Ping Zhao, zhaop@swu.edu.cn.

RNA-mediated knockdown of *JHAMT* in *D. melanogaster* did not result in the disruption of metamorphosis, while upregulation of *JHAMT* culminated in a pharate adult lethal phenotype (17). In *Tribolium castaneum*, RNA interference of functional *JHAMT* in the third instar has been observed to induce precocious metamorphosis although, phenotype rescue was achieved through the application of a JH analogue (23). These findings suggest that JHAMT plays a critical role in JH biosynthesis, mostly as a rate-limiting enzyme in most insects, and disruption of JHAMT activity is concomitant with lethality and/or failure of normal viable adult formation. As JHAMT is insect-specific, inhibition of this enzyme is deemed to be a feasible strategy for the development of novel insect growth regulators or bioinsecticide (16, 24–26).

To date, the characterization and physiological function of JHAMTs have been documented. However, information on the three-dimensional properties, specificity of ligand-binding interactions, and catalytic mechanism of this enzyme is woefully absent. Therefore, we present this report on three-dimensional structures for JHAMT from *B. mori*, as an apoenzyme, in a binary complex with the substrate SAH and as a JHAMT·SAH·MF ternary complex. Overall structural comparisons reveal a unique ligand-induced conformational change that facilitates accommodation of the ligands. Structural and biochemical analyses also allowed the ultrafine definition of the binding properties of JHAMT with the cofactor and the product, thus providing further insights into the catalytic mechanism of JHAMT. These findings also provide a strong basis for the discovery and development of specific JHAMT inhibitors as insect growth regulators or insecticides.

Results

Methylation activity of JHAMT homologs from B. mori

The first JHAMT gene, namely *JHAMT1*, was initially characterized in *B. mori* adults, and subsequently homologous genes encoding a putative methyltransferase were identified in larvae (16, 27). Currently, five homologues, (*JHAMT2*–*JHAMT6*) were observed in Blast searches of the SilkDB (https://silkdb.bioinfotoolkits.net/main/species-info/-1) and NCBI (https://www.ncbi.nlm.nih.gov/) databases. These encoded proteins were predicted to have a molecular mass of approximately 32 kDa and share 37 to 42% sequence identity (65–70% sequence similarity) compared with JHAMT1 (Fig. S1*A*). Furthermore, JHAMT proteins in *B. mori* contain a conserved SAM-binding motif (E/DXGXG/AXG) common within SAM-dependent methyltransferases (28) (Fig. 1*A*). To investigate whether these putative JHAMTs proteins exert methyltransferase activity by introducing a methyl group to the juvenoid acids *in vitro*, six *JHAMT* homologue genes were cloned from the *B. mori*. cDNA and heterologously expressed as N-terminal hexahistidine fusion proteins in *Escherichia coli*. Reversed-phase high-performance liquid chromatography (RP-HPLC) methyltransferase assays were conducted using FA as a substrate (Fig. 1*B*). It was found that when purified JHAMT1 or JHAMT2 was incubated with FA samples and 0.5 mM SAM, a new major peak was observed in the reaction

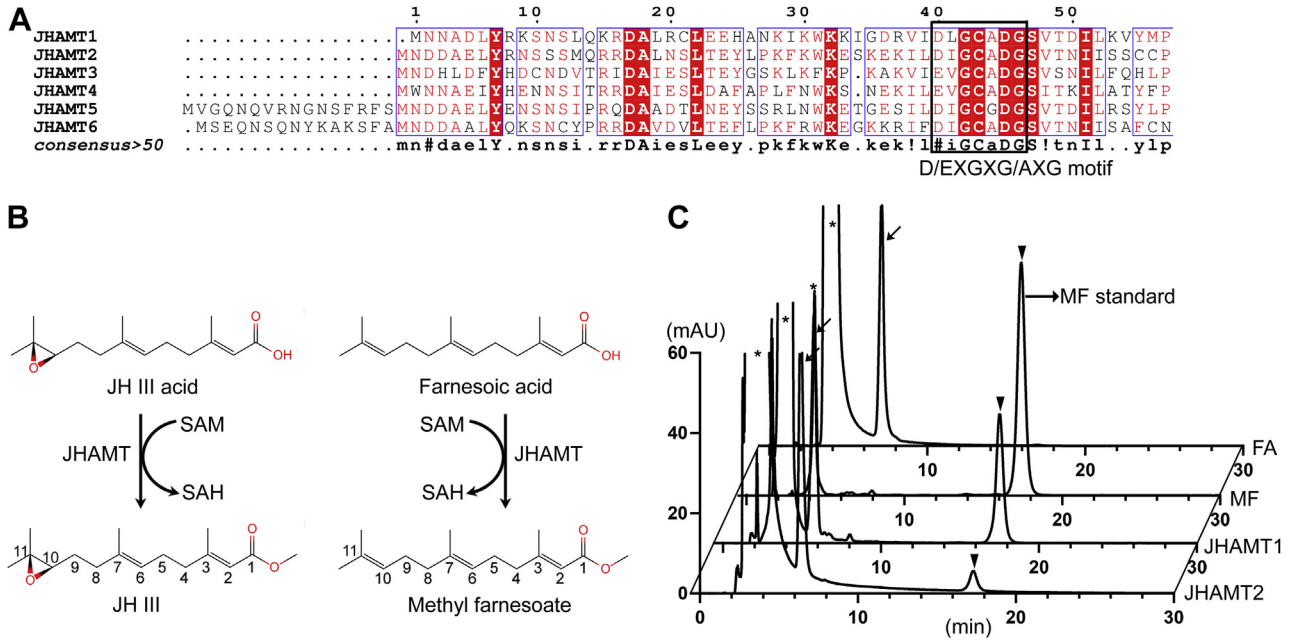

Figure 1. The homologs of *B. mori* JHAMT and its activity. *A*, multiple-sequence alignments of *Bombyx mori* JHAMT1 (BMSK0007003.1), JHAMT2 (BMSK0004751.1), JHAMT3 (BMSK0007002.1), JHAMT4 (BMSK0007001.1), JHAMT5 (XP_004929488.4), and JHAMT6 (XP_004933576.1). The SAM binding motif was marked with a *rectangular frame*, and the position of catalytic residue was marked with *red star*. The complete sequence alignment is provided in Figure S1, and the alignments were performed with *MultAlin* (41) and *ESPript* (42). *B*, the biosynthesis pathway from juvenoid acids (FA/JHA III) to juvenile hormone. *C*, RP-HPLC analyses of FA metabolites generated with recombinant *B. mori* JHAMT1 and JHAMT2 *in vitro*. Vertical axes represent UV absorption at 217 nm. *Arrow* and *arrowhead* indicate the FA and MF peaks, respectively; *Asterisks* indicate unidentified peaks originated from CH3CN used for sample preparation.

traces. The retention times of FA metabolites and known standards are summarized in the Figure 1*C*. Interestingly, the activity of JHAMT2 was appreciably lower than that of JHAMT1, and corresponding metabolite peaks were absent in reaction traces in the presence of JHAMT3, 4, 5, and 6 (Figs. 1*C* and S1*B*). These findings suggest that *JHAMT1* and *JHAMT2* represent the functional SAM-dependent methyltransferases toward the juvenoid acids (FA) encoded in silkworms.

Overall structure of JHAMT

The phase of JHAMT was determined by single-wavelength anomalous dispersion using selenomethionine (SeMet) substituted protein of *B. mori* JHAMT3 (PDB: 7V2S, Table S1, unpublished data), which contains two molecules in the asymmetric unit, and its electron density maps showed clear features of secondary structural elements (Fig. S2). The apo-JHAMT2 structure was determined at 2.95 Å resolution by molecular replacement phasing using the SeMet-JHAMT3 structure as the search model. Relevant data collection and refinement statistics are given in Table 1. As indicated in Figures 2*A* and S3*A*, JHAMT2 is structurally organized into a classical Rossman-fold core domain comprised of a seven-stranded β-sheet surrounded by six α-helices (α1–α5 and α8). Of these, helices α1, α2, and α3 reside on one side of the β sheet, while α4, α5, and α8 are juxtaposed to the opposing side. This Rossman-fold domain is the convention for protein architecture within methyltransferases (28) and forms the cofactor-binding domain. Interestingly, two augmentations of the Rossman-fold core allow distinction between JHAMTs. One permutation is an insertion composed of helices α7 and α8 located between strands β6 and β7 (residues Phe^{207}–Ala^{254}). The second conformer carries an insertion between strand β5 and helix α8 of the core fold (residues Met^{145}–Asp^{179}) of two helices α6 and α7 and a long flexible linker region between helices α7 and α8. These two insertions function as a "cap" located above the cofactor-binding domain and derive selective substrate binding by the enzyme (namely substrate-binding domain). The two domains are interspersed by a wide cleft that constitutes the binding site for cofactor and substrate (Fig. S3, *B* and *B′*). A search of Dali structural database (29) revealed several methyltransferases that are architecturally similar to JHAMT in the cofactor-binding domain, but are significantly diverse in the substrate-binding domain (Fig. S4, *A*–*F* and *H*), which further emphasized the functional role of this structural element. Moreover, superposition of JHAMT2 against these structures yields an overall root mean square deviation (RMSD) in the range of 2.8 to 16.7 Å over approximately 100 to 250 C_α atoms (Fig. S4*G*).

Symmetry operation showed that JHAMT2 forms a non-covalently linked homodimer with a total surface area of approximately 1128 Å^2 (Fig. 2*B*). Gel filtration chromatography also suggests that the eluted JHAMT2 exists as a dimer in solution with an apparent molecular weight of 69 kDa calculated from the calibration curve (Fig. S3*C*). Thus, the β-hairpin β5-β6-β7 geometry of the cofactor-binding domain in each subunit when two asymmetric units are orientated back to back forms a double-layered β-sheet at the center (Fig. 2, *B* and *C*). Notably, the linker region between helices α7 and α8

Table 1
Data collection, phasing, and refinement statistics

	JHAMT2 apo (PDB 7EBS)	JHAMT2·SAH (PDB 7EBX)	JHAMT2·SAH·MF (PDB 7EC0)
Data collection			
Space group	$P3_212$	$P4_322$	$P12_11$
Cell dimensions			
a, *b*, *c* (Å)	99.58, 99.58, 70.61	102.15, 102.15, 102.14	82.46, 101.20, 103.36
α, β, γ (°)	90, 90, 120	90, 90, 90	90, 93.5, 90
Molecules per asymmetric unit	1	1	6
Resolution range (Å)[a]	86.24–2.95 (3.06–2.95)	45.73–2.90 (2.95–2.90)	72.25–2.49 (2.63–2.49)
No. unique reflections	8562 (850)	12,618 (603)	58,792 (8516)
R_{merge}[b]	0.048 (0.66)	0.082 (0.908)	0.056 (0.734)
$I/\sigma(I)$	30.7 (2.3)	42.9 (1.8)	18.2 (2.6)
Completeness (%)	99.7 (99.9)	100.0 (100.0)	99.4 (99.1)
Redundancy	6.7 (7.1)	20.5 (17.0)	6.9 (7.1)
Refinement			
Resolution (Å)	86.24–2.95 (3.03–2.95)	45.73–2.90 (2.98–2.90)	72.25–2.49 (2.56–2.49)
R-factor[c]/R-free[d] (%)	23.6/28.1	25.2/29.2	24.5/29.3
No. atoms			
Protein	2140	2137	12,272
Ligand/ion	0	26	220
Water	0	6	24
Mean B factors (Å2)	103.68	112.03	68.59
Ligand B factors (Å2)		86.76	63.45
R.m.s deviations			
Bond lengths (Å)[e]	0.004	0.003	0.003
Bond angles (°)[e]	1.278	1.224	1.200
Ramachandran plot			
Most favored (%)	95.70	94.42	95.74
Additional allowed (%)	3.12	3.98	3.85

[a] Values in parentheses are for the highest resolution shell.
[b] $R_{merge} = \sum_{hkl}\sum_i|I_i(hkl) - \langle I(hkl)\rangle| / \sum_{hkl}\sum_i|I_i(hkl)|$, where $I_i(hkl)$ is the intensity of an observation and $\langle I(hkl)\rangle$ is the mean value for its unique reflection; Summations are over all reflections.
[c] $R - factor = \sum_h||Fo(h)| - |Fc(h)|| / \sum_h|Fo(h)|$, where Fo and Fc are the observed and calculated structure-factor amplitudes, respectively.
[d] R-free was calculated with 5% of the data excluded from the refinement.
[e] Root-mean square-deviation from ideal values.

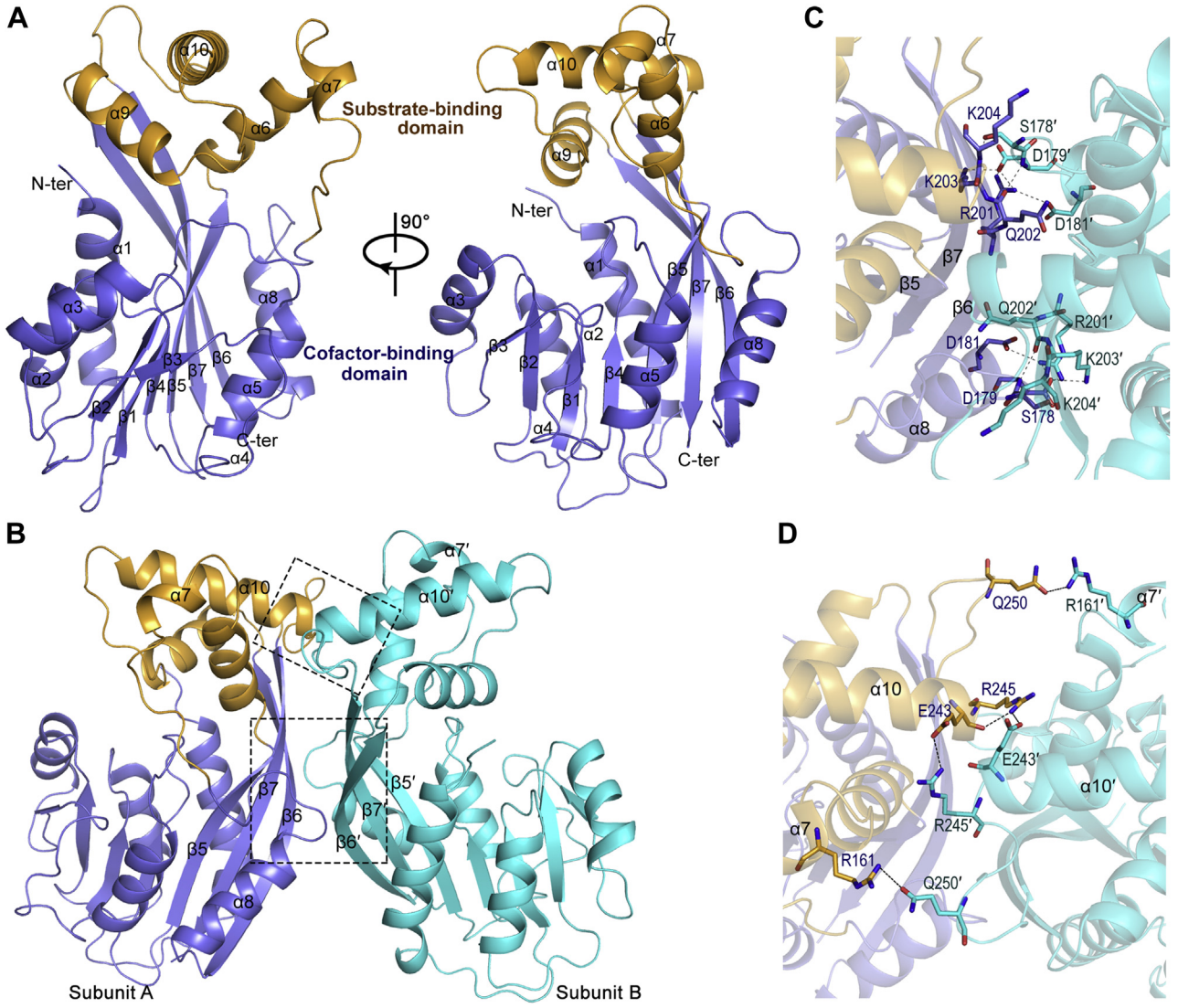

Figure 2. The overall structure of *B. mori* JHAMT. *A*, cartoon representation of the JHAMT2 apo form in two orientations rotated by 90°. Slate, cofactor-binding domain; *Orange*, substrate-binding domain. *B*, schematic representation of the JHAMT2 dimer. The two dimeric interfaces between subunits were highlighted with dashed frame. *C*, the residues from cofactor-binding domain and (*D*) the residues from substrate-binding domain involved in the formation of hydrogen contacts and salt bridges at the dimeric interface are shown in *sticks*.

within the substrate-binding domain also forms interactions with the β6-β7 hairpin of the symmetric subunit. Helix α10 and the loop region that intersperses α10 and β7 of the substrate-binding domain protruding toward the symmetric unit are in proximity to the second molecule of the homodimer through intermolecular hydrogen bonds and salt bridges (Fig. 2, *B* and *D*).

The JHAMT·SAH complex and the cofactor-binding site

SAM is an essential cofactor for methyltransferase catalysis in providing a CH_3 group (18). To identify the pattern of cofactor binding to the *B. mori* enzyme, JHAMT was cocrystallized with SAM, and the three-dimensional structure was derived at a resolution of 2.90 Å. In this complex, as the methyl group of SAM is highly reactive at the sulfonium center, its corresponding product, SAH, is observed in the hydrophilic cleft within the cofactor-binding domain being stabilized through interactions with residues from within the loop regions between β2–α3, β3–α4, and β4–α5 (Fig. 3, *A* and *B*). As shown in Figure 3*C*, the adenine ring is enclosed by a relatively hydrophobic cavity defined by the residues Val^{69}, Ile^{93}, Trp^{116}, and Ile^{117}, with the adenine moiety NH_2 groups and N1 atom stabilized through hydrogen bonds to the side chain of Asp^{92} (OD1) and the main-chain nitrogen of Ile^{93}. The adenosine ribose of SAH forms a hydrogen bond with the side-chain oxygen of Thr^{113} (OG1). Furthermore, the methionine moiety fits into the relatively wider part of the cleft with the positively charged amino nitrogen forming two hydrogen bonds with the main-chain atoms of Gly^{43} and Phe^{111}, respectively. A comparison of structure and residues shows that JHAMT1 and JHAMT2 are equivalent in the SAH-binding site (Fig. S5). Thus, further verifications of residues associated with cofactor binding in the binary complex were

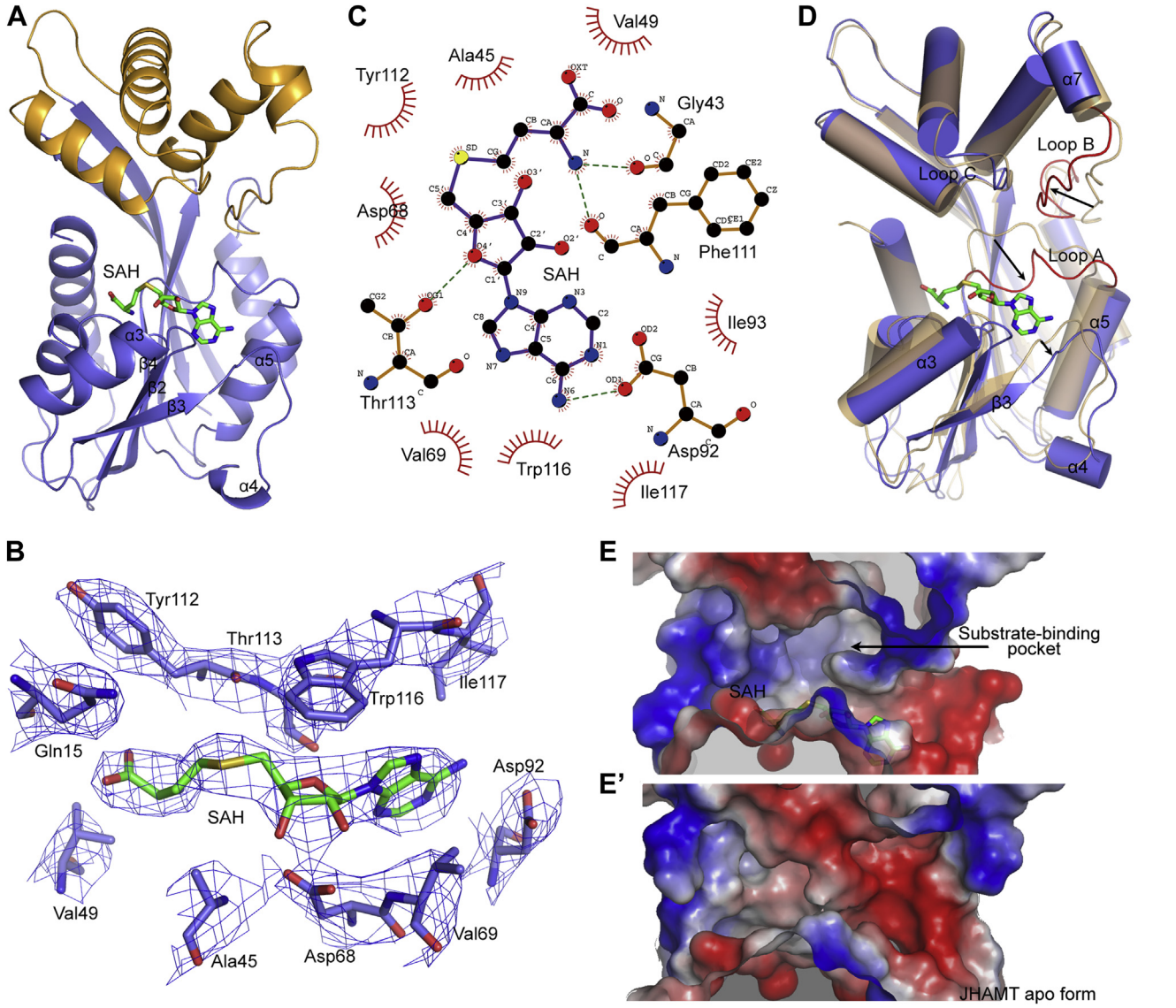

Figure 3. Structure of JHAMT2·SAH complex and cofactor-binding site. *A*, cartoon representation of the JHAMT2·SAH complex. The cofactor SAH is shown as *green* stick. *B*, the 2Fo − Fc omit map around the SAH molecule is shown in mesh contoured at 1.0 σ. *C*, schematic representation of interactions between JHAMT2 and SAH analyzed using the *LigPlot*$^{+}$ program (43). *D*, superimposition of the overall structure of the SAH-bound JHAMT2 (slate) and that of apo-JHAMT2 (sand). The loop regions with conformational changes are emphasized with *red* color. *E*, the potential surface of cofactor-binding pocket in the SAH-bound JHAMT2 and (*E*′) the corresponding site in the apo-JHAMT2.

assessed through deleterious mutation of residues within JHAMT1/2 involved in hydrogen bonding to cofactor and assessment of binding affinities in fluorescence-binding assays. As indicated in Table 2, the binding affinities of JHAMT1 and JHAMT2 for SAM are 38.67 μM and 42.63 μM, respectively. In contrast, the K_d values for mutants $D^{91}A$ ($D^{92}A$ in JHAMT2) and $T^{112}A$ ($T^{113}A$ in JHAMT2) decreased in the order of *ca* ∼4 to 6-fold, which imply that these residues are crucial for cofactor interactions. Moreover, multiple-sequence alignment shows that the SAM/SAH-binding site is highly conserved at

Table 2
The K_d value of *B. mori* JHAMTs wild-type and its mutants with SAM and FA

Enzyme	K_d value for SAM (μM)	Enzyme	K_d value for FA (μM)
JHAMT1	38.67 ± 3.42	JHAMT1	0.20 ± 0.04
JHAMT1-$D^{91}A$	229.50 ± 18.10	JHAMT1-$Q^{14}A$	0.27 ± 0.05
JHAMT1-$T^{112}A$	190.52 ± 12.75	JHAMT1-$Q^{14}E$	0.19 ± 0.04
		JHAMT1-$H^{114}A$	0.39 ± 0.06
JHAMT2	42.63 ± 5.83	JHAMT2	0.21 ± 0.04
JHAMT2-$D^{92}A$	260.70 ± 18.07	JHAMT2-$Q^{15}A$	0.31 ± 0.04
JHAMT2-$T^{113}A$	143.80 ± 9.91	JHAMT2-$Q^{15}E$	0.21 ± 0.03
		JHAMT2-$H^{115}A$	0.35 ± 0.05

Binding affinities were determined in 20 mM Tris-HCl, pH 8.0, 200 mM NaCl, at 25 °C (data are represented as the mean ± s.d., n = 3 independent experiments).

the primary sequence through evolutionary conservation of the cofactor-binding domain within JHAMTs (Fig. S6).

While there are overall structural similarities between the apoenzyme and JHAMT2·SAH complex, superposition of these structures yields an RMSD of 1.39 Å over 228 Cα atoms and reveals that a profound conformational change in the protein occurs upon forming interactions with SAH. Most remarkably, α3 helical rigidity shifts toward SAH molecule, the β3–α4 loop region, and helix α5 shift about 2.2 and 1.8 Å, respectively, away from SAH, providing sufficient three-dimensional space to accommodate the adenine moiety of the cofactor (Fig. 3*D*). Additionally, the loop A region formed by residues over Thr^{113}–Ile^{117} in between β4 and α5 shifts about 7.0 Å toward the adenine moiety that packs against SAH. These conformational changes lead to a wider cleft for any incoming SAH molecule. Furthermore, the loop B region formed over residues Ile^{167}–Tyr^{175} between helices α7 and α8 shifts about 6.2 Å toward the SAH-binding site of the complex, despite the absence of any direct interaction formed with the cofactor. Intriguingly, the significant conformational change of loop A, together with the shift of loop region B, contributes to a wide hydrophobic cavity near the SAH molecule with the rearrangement of amino acid residues considered to be rudimentary for substrate-binding pocket formation for the approaching hydrophobic substrate during initial substrate recognition events (Fig. 3, *E* and *E*′).

Structure of the JHAMT·SAH·MF ternary complex and the substrate-binding pocket

There are six molecules in an asymmetric unit in the JHAMT·SAH·MF structure, in which five of the six subunits displayed highly similar overall architecture with an overall RMSD in the range of 0.21 to 0.25 Å over approximately 230 Cα atoms (Fig. S7*A*). However, one subunit was structurally dissimilar having distinct flexibility in the absence of ligands (Fig. S7*A*). In each ligand-bound subunit, the electron density of the SAH molecule and the terpenoid backbone of MF are well defined, whereas the ester moiety of MF is not visible in the density map, presumably due to its low occupancy and/or higher mobility (Fig. 4*A*). In the ternary complex, the SAH molecule is located in a deep cleft of the cofactor-binding domain, and one molecule of MF is bound in the hydrophobic cavity located vertically above the Sδ atom of the SAH molecule (Fig. 4*B*). The substrate-binding pocket presents an irregular conical shape, with a narrow opening and a wide hole. Polar residues Gln^{15}, His^{115}, and the aromatic residue, Trp^{116}, form an alkaline neck of the pocket. Amino acid residues Leu^{142}, Val^{147}, Phe^{148}, and Phe^{151} within helix α6, Ile^{167}, Phe^{170}, Ile^{171} of helix α7, together with Val^{220} and Pro^{222} in the loop between α9 and α10, form a hydrophobic broad cavity (Fig. 4*C*). To fit in the pocket, the MF molecule assumes an S-shape structure, which has a similar conformation as that observed for JH bound to JH-binding protein (30). Specifically, the ester side of MF is poised at the entrance to the substrate-binding pocket and mainly stabilized by residues Gln^{15} and His^{115} through hydrogen bonds and van der Waals interactions. The carbonyl oxygen of the ester forms a direct hydrogen bond with the Nε2 atom from His^{115} over a short distance of 2.8 Å, and the oxygen of methoxy group is within 4.0 Å of two potential hydrogen bonds acceptors in the amino groups of Gln^{15} and His^{115}. The terpenoid backbone of MF is confined in a hydrophobic sidewall and makes contact with the side chain of Trp^{116}, Met^{145}, and Val^{147} in helix α6 and Val^{220} and Pro^{222} in the loop between helices α9 and α10. Besides, the isopropyl tail of MF stretches to the base of the hydrophobic pocket and is fixed by the CH-π staking in between methyl groups attached to C11 with the aromatic rings of Phe^{148}, Phe^{151}, Phe^{170}, Phe^{223}, and van der Waals interactions with the hydrophobic side chains of Ile^{167} and Ile^{171} (Fig. 4*C*). Similarly, in the structural model of JHAMT1, a substrate-binding pocket that is comparable to that within JHAMT2, except for the substitution of Thr^{144} for Met^{145}, is composed of conserved residues (Fig. 4*C*).

To verify the functional relevance of specific amino acid contacts within JHAMT considered of importance to binding interactions with ligand molecules, mutational analyses and *in vitro* activity assays were performed using JHAMT1 as it displays higher native activity than JHAMT2. The kinetic analyses revealed that the K_m and k_{cat} values of JHAMT1 were 42.28 ± 3.73 μM and 0.92 ± 0.02 min^{-1} toward cofactor SAM and 11.05 ± 1.64 μM and 1.14 ± 0.06 min^{-1} toward FA. As shown in Table 3, within the detection limits, the replacement of Gln^{14} with Ala/Glu and of His^{114} with Ala resulted in a loss of methylation activity with FA, and the binding affinity (K_d value) of these mutants toward FA was comparable to that of the wild-type (Table 2), suggesting the crucial roles of the Gln^{14} and His^{114} in JHAMT catalysis. In addition, the replacement of any Trp^{115}, Thr^{144}, Val^{146}, Ile^{219}, or Pro^{221} that normally stabilizes the terpenoid backbone of MF with Ala had a pronounced effect on the trans-methylation activity. The K_m values of mutated forms $W^{115}A$, $T^{144}A$, $I^{146}A$, $I^{219}A$, or $P^{221}A$ for FA were between 4- and 7-fold lower affinity compared with the wild-type enzyme. Similarly, k_{cat} values of these variants were significantly slower, being between 10 and 70% the rate of the wild-type enzyme, and the ratio of k_{cat}/K_m for FA substrate decreased by approximately 6 to 55-fold (*cf.* wild-type; Table 3). The individual contributions of Phe^{147}, Tyr^{150}, Phe^{169}, Phe^{222}, Ile^{167}, and Ile^{171}, which form contacts with the isopropyl tail of MF, were also assessed through mutational analyses and activity assays (Table 3). Of these the K_m values of $F^{169}A$ and $F^{222}A$ forms of JHAMT for FA were significantly higher, while the $F^{147}A$ and $Y^{150}A$ forms showed little change when compared with the wild-type enzyme. Interestingly, all variant forms of JHAMT display lower k_{cat} values, which are decreased by as much as 70% when compared with the wild-type enzyme, equivalent to a 9 to 100-fold decrease in catalytic efficiency (Table 3). These findings demonstrate that the hydrophobic interaction network can not only fix the substrate but also participate in the catalytic mechanism. Moreover, multiple-sequence alignment revealed that the catalytic residues $Gln^{14/15}$ and $His^{114/115}$ are strictly

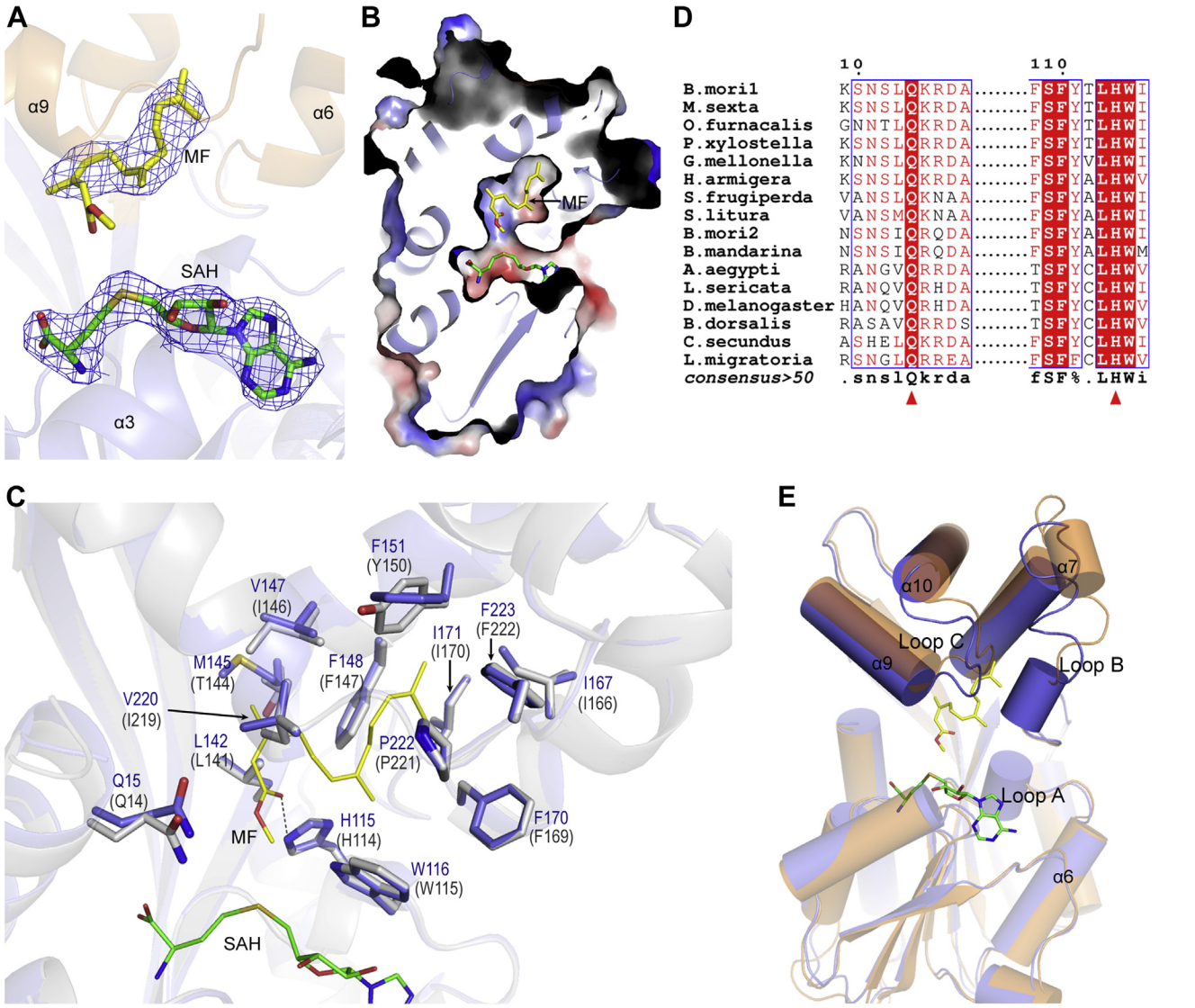

Figure 4. Structure of ternary complex JHAMT2·SAH·MF. *A*, 2Fo − Fc omit map contoured at 1.0 σ around the SAH and MF molecules in the JHAMT2·SAH·MF complex. *B*, surface representation of JHAMT2·SAH·MF complex. The irregular conical-shaped pocket within JHAMT is indicated. The MF molecule (shown as *yellow stick*) is located in the hydrophobic cavity and the SAH molecule (shown as *green stick*) is located in the adjacent pocket. *C*, the interaction of MF molecule with adjacent residues of JHAMT. Residues of JHAMT2 and JHAMT1 involved in the MF binding are shown in sticks and the hydrogen bonds are *black dashed lines*. JHAMT2 and JHAMT1 are shown in slate and *gray*, respectively. MF and SAH are colored with *yellow* and *green*, respectively. *D*, multiple-sequence alignment of JHAMTs from *B. mori* and other insects show the strictly conserved catalytic pair (*red triangles*). *B. mori*1, JHAMT1 from *B. mori*; *M. sexta*, *Manduca sexta*; *O. furnacalis*, *Ostrinia furnacalis*; *P. xylostella*, *Plutella xylostella*; *G. mellonella*, *Galleria mellonella*; *H. armigera*, *Helicoverpa armigera*; *S. frugiperda*, *Spodoptera frugiperda*; *S. litura*, *Spodoptera litura*; *B. mori*2, JHAMT2 from *B. mori*; *B. mandarina*, *Bombyx mandarina*; *A. aegypti*, *Aedes aegypti*; *L. sericata*, *Lucilia sericata*; *D. melanogaster*, *Drosophila melanogaster*; *B. dorsalis*, *Bactrocera dorsalis*; *C. secundus*, *Cryptotermes secundus*; *L. migratoria*, *Locusta migratoria*. The complete sequence alignment is provided in Figure S6. *E*, superimposition of the overall structure of the SAH- and MF-bound JHAMT2 (slate) and that of SAH-bound JHAMT2 (*orange*).

conserved in the JHAMT family (Fig. 4*D*). Thus, these pairs of amino acids are of critical importance in the determination of JHAMT-like protein methyltransferase activity. Moreover, except for Thr[144], residues that form the hydrophobic cavity and make contacts with the substrate molecule are constitutive or only conservatively substituted within the JHAMT family in insects (Fig. S6).

Superimposition of JHAMT·SAH complex with the JHAMT·SAH·MF ternary complex yields an RMSD of 0.65 Å over 228 Cα atoms and reveals that a further significant conformational change occurs within JHAMT in the presence of MF. Upon the interaction of MF with JHAMT·SAH, significant deviations are observed in the substrate-binding domain (Fig. 4*E*), wherein helices α9 and α10, together with loop C in between helices α9 and α10, are rigidly shifted toward the center cleft, promoting residues Val[220], Pro[222], and Phe[223] to move 1.6 Å, 3.1 Å, and 2.8 Å, respectively, toward the MF carbon skeleton. Furthermore, loop B between α6–α7 and α7–α8 becomes orientated toward the MF molecule, with residues Ile[167] and Phe[170] being approximately 7.3 Å and 3.6 Å, respectively, in proximity to the MF molecule (Fig. S7*B*). These conformational changes lead to further compaction within the substrate-binding domain to form a deep substrate-binding pocket that prevents hydrophobic substrate solvation.

Table 3
Kinetic parameters of the wild-type JHAMT1 and its mutants toward farnesoic acid

Enzyme	K_m (μM)	k_{cat} (min^{-1})	k_{cat}/K_m (mM^{-1} min^{-1})
JHAMT1-WT	11.05 ± 1.64	1.14 ± 0.06	102.89 ± 5.30
$Q^{14}A$	ND	ND	ND
$Q^{14}E$	ND	ND	ND
$H^{114}A$	ND	ND	ND
$W^{115}A$	73.32 ± 7.74	0.13 ± 0.01	1.83 ± 0.10
$T^{144}A$	40.42 ± 6.54	0.78 ± 0.04	19.33 ± 0.94
$I^{146}A$	67.83 ± 7.16	0.50 ± 0.02	7.33 ± 0.29
$F^{147}A$	20.42 ± 1.25	0.02 ± 0.001	1.08 ± 0.02
$Y^{150}A$	23.82 ± 4.45	0.11 ± 0.01	4.39 ± 0.33
$V^{166}A$	291.60 ± 21.32	1.07 ± 0.17	3.66 ± 0.57
$F^{169}A$	112.60 ± 9.98	0.84 ± 0.03	7.45 ± 0.26
$I^{170}A$	45.01 ± 7.67	0.18 ± 0.01	4.02 ± 0.24
$I^{219}A$	40.23 ± 3.04	0.09 ± 0.002	2.30 ± 0.06
$P^{221}A$	50.32 ± 3.47	0.41 ± 0.04	8.08 ± 0.21
$F^{222}A$	40.42 ± 6.46	0.46 ± 0.04	11.41 ± 0.89

Activities were determined in 50 mM HEPES buffer, pH 8.0, with 1 mM SAM, at 25 °C (data are represented as the mean ± s.d., n = 3 independent experiments)
Abbreviation: ND, not detected

Putative catalytic mechanism of JHAMT

The binding of products SAH and MF at the active site of JHAMT provides a suitable model for study of the FA/JHA substrate interactions with the enzyme. Thus, based on the SAH-bound binary and JHAMT·SAH·MF ternary complexes, respectively FA/JHIIIA and SAM were modeled into the structure of JHAMT. These molecules were positioned within the hydrophobic cavity by superposition of the terminal portion of MF and the carboxyl group extended to the methyl group of the modeled SAM (Fig. 5, *A* and *B*). In the active site, Gln^{14} and His^{114} (*B. mori* JHAMT1) are positioned to anchor the carboxyl group of the substrate. The Nε2 of His^{114} forms hydrogen bonds with the carbonyl and hydroxyl group of the substrate, and the Gln^{14} Nε2 atom could form a hydrogen bond with the hydroxyl group of the substrate. The mutations of $Q^{14}E$, $Q^{14}A$, and $H^{114}A$ inactivate the enzyme, but have no effect on the substrate binding (Tables 2 and 3), indicating that the Gln/His pair is involved in the JHAMT catalysis. Histidine is a Schiff base as its side chain proton readily dissociates under neutral or alkaline conditions. The mutations of the $H^{114}Q$, $H^{114}F$, and the double mutant $Q^{14}H/H^{114}Q$ (swapping the location of Gln and His) resulted in the loss of methylation activity with FA (Fig. 5*C*), suggesting that the essential His^{114} needs to be present with the appropriate location and geometry to deprotonate the substrate. In addition, the replacement of Gln by basic residue His in JHAMT1 ($Q^{14}H$) also abolished the methylation activity in JHAMT1, and the mutation of Thr to Gln in the inactive JHAMT isoform, JHAMT3 (JHAMT3-$T^{15}Q$), recovered the methyltransferase activity with FA (Fig. 5*C*). These results indicated that Gln is a crucial residue in the JHAMT catalysis. The Gln presumably anchors the carboxyl group of the substrate in the correct orientation, to position the hydroxyl group proximal to the methyl group of SAM. The closeness between the hydroxyl group and the CH_3 donor coupled to polarity within the active site is a prerequisite for methylation. Consequently, during catalysis, His^{114} in JHAMT acts as a proton acceptor that causes deprotonation of the substrate –OH group. Subsequently, the $-O^-$ group of JHA/FA is presumed to make a nucleophilic attack on the methyl group of SAM. Concomitantly, the CH_3 of the SAM moiety is a leaving group from the Sδ onto the susceptible position of the deprotonated hydroxyl group. Thus, the carboxyl group is converted to an ester group, producing and MF and SAH (Fig. 5*D*).

Discussion

In this study, two functional homologs JHAMT1 and JHAMT2, obtained from *B. mori*, were identified and enzymatically characterized in terms of methylation of farnesoic acid (FA) to methylfarnesoate (MF), albeit with the activity of JHAMT2 being significantly lower than that of JHAMT1. The crystal structure of JHAMT2 was determined, thereby providing the first recorded three-dimensional structure of the enzyme from insects. The *B. mori* JHAMT structure is composed of a substrate-binding domain and Rossman-fold cofactor-binding domain that is relatively conserved across other classes of SAM-dependent methyltransferases, despite some disparity between residues that contribute to the domain structure (28, 31, 32). Owing to significant diversity in the shape, size, and chemistry of methyltransferase ligands, the structure of the substrate-binding region varies considerably across individual methyltransferases (28). Indeed, JHAMT shows a novel structural fold compared with that of other reported SAM-dependent methyltransferases, which presumably reflects highly specific binding of JHA (Fig. S4).

To further elucidate the determinants of substrate recognition, cocrystallization studies were attempted for JHAMT with the cofactor (SAM), substrate (FA), and product (MF), respectively, with the crystallization trail of JHAMT with substrate/product and cofactor (SAM and FA, SAH and MF). Finally, the complex of JHAMT with SAM and the ternary complex with SAH and MF were solved, and these structures greatly enhanced our present understanding of substrate recognition and catalytic mechanism of JHAMT. Interestingly, the binding of SAH induced a significant conformational change around the SAH-binding site that facilitates the accommodation of the cofactor. Simultaneously, the induced fit promoted a significant rearrangement of residues in the substrate-binding domain, forming a wide hydrophobic cleft that facilitated incoming substrate molecule binding (Fig. 3, *E* and *E*′). The hydrophobic cleft was rudimentary of the substrate-binding site upon initial recognition and underwent further conformational changes to finally form a deep conical-shaped pocket upon interaction with MF (Fig. 4, *B* and *E*). These progressive conformational changes indicated that JHAMT would combine with the cofactor first with substrate interactions being secondary to the process of ligand accommodation. This explained why crystals of JHAMT protein with the substrate FA or the product MF were unobtainable in the absence of the cofactor.

From the ternary structure of JHAMT bound to cofactor and product, a substrate-binding pocket incorporating a deep hydrophobic cleft and an alkaline groove entrance was observed. The amino acid pair of Gln^{14} and His^{114} (*B. mori* JHAMT1) located at the entrance of the substrate-binding

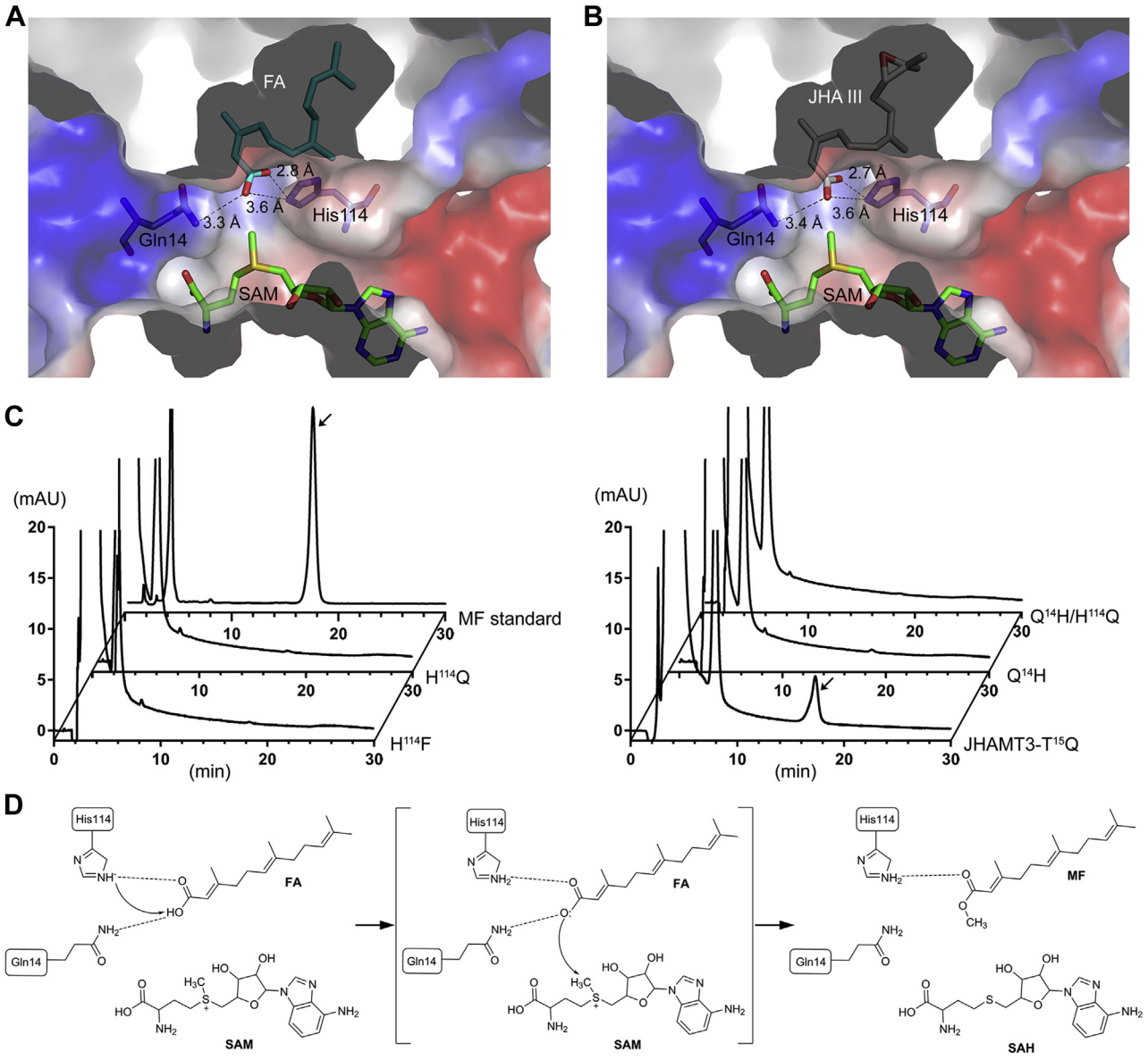

Figure 5. Catalysis mechanism of JHAMT enzyme. *A*, model-built substrate FA and (*B*) JHA III and SAM are shown in a cutaway of a space-filling surface model to illustrate their reaction state of JHAMT. The FA/JHA III was positioned by aligning its hydrophobic skeleton to that of MF. FA, JHA III, and SAM are colored with *cyan*, *gray*, and *green*, respectively. The proposed hydrogen bonds are *black dashed lines*. *C*, RP-HPLC analyses of FA metabolites generated with JHAMT1 mutants and JHAMT3-T^{15}Q mutant *in vitro*. Vertical axes represent UV absorption at 217 nm. *Arrow* indicates the MF peaks. *D*, proposed reaction mechanism for methyl transfer in JHAMT enzymes.

pocket was prerequisite for catalysis and strictly conserved across JHAMT orthologs (Fig. 4, *C* and *D*). Thus, this amino acid pair can be regarded as an important feature for the determination of whether a JHAMT-like protein has methyltransferase activity. Moreover, sequence alignment of JHAMT homologs in *B. mori* showed that these two key residues are conserved in the JHAMT1 and JHAMT2, but the Gln is replaced by Thr or Pro in other JHAMT isoforms (Fig. 1*A*). This observation aided in the explanation of the reason that *B. mori* JHAMT 3, 4, 5, and 6 share high sequence similarity with JHAMT1 and JHAMT2 but do not display methyltransferase activity. In the cavity of the substrate-binding pocket, there is a slight opening space in the vicinity of the methyl groups attached to C7 and C11, and the groups were substituted by ethyl group in the JHA I or half-substituted (C11 position) by ethyl group in JHA II (Figs. 4*B* and S7*C*). This structural feature within the substrate-binding pocket can plausibly explain the catalytic efficiency of juvenoid acids for *B. mori* JHAMT in the order of JHA I > JHA II > JHA III (16), as filling these open spaces by a slightly branched methyl group could result in closer contacts between the ligand molecule and the hydrophobic wall. Meanwhile, this relationship between structure and function also applies to the fact that both *B. mori* JHAMT and *D. melanogaster* JHAMT are highly specific to juvenoid acids, FA and JHA III, but not unbranched fatty acids (16, 17). In the JHAMT·SAH·MF complex, the mode of binding of SAH and MF represented the protein structural state of JHAMT at the end of the

transmethylation. In this state, the original hydrogen bond between the $Gln^{14/15}$ and $His^{114/115}$ with the hydroxyl group of the substrate (FA) would be broken upon methylation. Thus, although the positions of terpenoid backbones were nearly identical for the five structures of MF molecules bound in the ternary complexes present in the crystal asymmetric unit, the positions of carbonyl groups were different from each other mainly due to lack of sufficient hydrogen bonds to stabilize these complexes (Fig. S7*D*). This might also explain why the electron density cloud of the carbonyl group of MF cannot be tracked. Furthermore, JHAMT is rate-limiting in JH biosynthesis and specific to insects, thus presenting an excellent target for the development of safe insect growth regulators (24, 26, 33). The three-dimensional structure of JHAMT and its ligand-bound complexes, combined with the detailed catalytic mechanism of JHA recognition by JHAMT, provides the opportunity to rationalize the computer-assisted design of inhibitors and further aids in the development of potent insect growth regulators or insecticides.

Experimental procedures

Protein expression and purification

The DNA fragments encoding the juvenile hormone acid methyltransferase *B. mori* (JHAMT1, 2) and its homologs were amplified by PCR and cloned into a pET28a-derived vector, respectively (Table S2). The constructs with an N-terminal hexahistidine tag were transformed into the *E. coli* BL21 (DE3) strain (Novagen), and the bacteria were cultured in TB medium at 37 °C. When the OD_{600} of the culture reached 1.0 to 1.5, the expression of JHAMTs was induced by the addition of 0.2 mM isopropyl-β-D- thiogalactopyranoside at 16 °C for 20 h. The cells were harvested by centrifugation at 6000*g* for 20 min and then were resuspended in binding buffer (20 mM Tris-HCl, pH 8.0, 200 mM NaCl). After high-pressure homogenization and centrifugation at 12,000*g* for 30 min, the supernatants were transferred into new centrifuge tubes and mixed with Ni^{2+}-NTA agarose resin (GE Healthcare) that had been equilibrated with binding buffer. The mixture was incubated at 4 °C for 1 h with rotation and then loaded on a column. The target protein was eluted with 300 mM imidazole buffer and then was loaded onto a HiLoad 16/60 Superdex 75 column (GE Healthcare) equilibrated with 20 mM Tris-HCl, pH 8.0, 50 mM NaCl. The purity of the eluted protein was estimated by sodium dodecyl-sulfate polyacrylamide gel electrophoresis, and the protein sample was stored at −80 °C. The mutant proteins were expressed, purified, and stored in the same manner as the wild-type protein.

Crystallization and data collection

Crystallization screens were set up at 16 °C by mixing equal volume of protein sample and reservoir solution, using the sitting-drop vapor-diffusion method. Crystals of JHAMT2 apoform were grown by mixing 1 μl of 7.5 mg/ml protein sample with equal volume of mother liquor (0.1 M Bis-Tris pH 5.5, 1 M ammonium sulfate, and 1% polyethylene glycol 3350) with the hanging-drop vapor-diffusion method. The crystals of SAH-bound complex were obtained by cocrystallizing JHAMT2 with 5 mM SAM in 0.1 M Bis-Tris pH 5.5, 1 M ammonium sulfate, and 1% polyethylene glycol 3350. The SAH and MF-bound protein complex was made by mixing the freshly purified JHAMT2 with 5 mM SAH and MF solution and incubating the mixture at 4 °C overnight. Crystals of JHAMT2·SAH·MF complex were harvested in a reservoir solution of 0.15 M DL-Malic acid pH 7.0, and 20% polyethylene glycol 3350. Crystals were flash-cooled in liquid nitrogen at 100 K for data collection using 20% glycerol in mother liquor as cryo-protectant for JHAMT2 and JHAMT2·SAH complex crystals and reservoir solution supplemented with 30% PEG400 reservoir solution as cryo-protectant for JHAMT2·SAH·MF ternary complex crystals. All diffraction data for single crystal was collected at a wavelength of 0.979 Å at Shanghai Synchrotron Radiation Facility, Shanghai Institute of Applied Physics, Chinese Academy of Sciences, using beamline BL 17U at 100 K with a DECTRIS Pilatus 36M CCD. Data processing and scaling were performed using the *HKL3000* package (34). The dataset statistics are shown in Table 1.

Structure solution and refinement

The initial phase of JHAMT was obtained from the SeMet-derivative JHAMT3 crystal by single-wavelength anomalous dispersion phasing method using the *AutoSol* program from *PHENIX* (Unpublished data). Relevant data collection and refinement statistics are given in Table S1. The crystal structure of JHAMT2 apo-form was determined by the molecular replacement method with *MOLREP* (35) in the *CCP4i2* suite (36) using the model of SeMet-JHAMT3 as the search model. Refinement was carried out by several rounds of maximum-likelihood-based refinement of individual coordinates and individual B factors using *REFMAC5* (37). After every round of refinement, the model was manually checked against Fo – Fc and 2Fo – Fc electron density maps in *Coot* (38). In addition, both the structures of the JHAMT2·SAH binary complex and the ternary complex with SAH and product were determined by the molecular replacement method using the refined JHAMT2 apo-form model. These structure models were also refined by the iterative refinement with *REFMAC5* (37) and the interactive rebuilding process in *Coot* (38). The overall assessment of model quality was performed using *MolProbity* (39). A summary of structure refinement statistics is provided in the Table 1. All structural figures were prepared with *PyMOL* (40).

Fluorescence measurements

A Hitachi F-7100 fluorescence spectrophotometer was used to measure emission fluorescence spectra, in a right-angle configuration with a 1 cm light-path quartz cuvette. The slit width was 5 mm for both excitation and emission. Considering the high content of tryptophan (1.4%) and tyrosine (4.3%) residues in *B. mori* JHAMT, we used an excitation wavelength at 280 nm to measure the intrinsic fluorescence of tryptophan side chain. A quartz-cuvette containing 2500 μl of protein sample (2 μM) was incubated for 2 min at 25 °C before

measurement. SAM (Sigma-Aldrich) at a final concentration of 0 to 1.5 mM was added to the protein sample, respectively, in the cofactor-binding affinity assay. FA at a final concentration of 0 to 0.1 mM was added to the protein sample, respectively, in the substrate-binding affinity assay. The reaction was started by adding substrate, and the fluorescence quenching data were recorded in the range 300 to 450 nm, with an excitation wavelength of 280 nm. Each reaction was repeated three times, and the K_d values were calculated with *GraphPad Prism 5.0*.

Enzymatic activity assays

The enzymatic activity of JHAMT was measured by quantifying the amount of product in the reaction, as described in previous studies, with some modification (16, 17). Briefly, in a 450 μl reaction mixture containing 50 mM HEPES, pH 8.0, recombinant JHAMT proteins were incubated for 2 min at 25 °C before measurement. To determine the kinetic parameters of JHAMT for FA, 500 μM SAM (Sigma-Aldrich) was added to the reaction mixture, and the reaction was triggered by adding 50 μl substrate FA (Echelon Bioscience) with different concentrations (0–300 μM). To determine kinetic parameters of JHAMT for SAM, 500 μM FA (Sigma-Aldrich) was added in each reaction system, and the reaction was started by adding SAM at different concentrations (0–400 μM). After incubation at 25 °C for 10 min (JHAMT1 wild type) or 60 to 120 min (JHAMT1 mutants), the reactions were stopped by the addition of 500 μl of CH_3CN (Honeywell). Under these conditions, the rate of product formation was linear during the reaction. The reaction mixture was centrifuged at 4000*g* for 30 min, and the top phase (150 μl) was transferred into a small vial for RP-HPLC analysis. The MF standard (Echelon Bioscience) was quantified by RP-HPLC analysis using various concentrations ranging from 0.15 to 80 μM. RP-HPLC was performed with Agilent 1290 HPLC system equipped with a Symmetry C18 column (5 μm, 4.6 mm × 150 mm; Waters). The column was equilibrated and eluted with 80% CH_3CN at a flow rate of 0.5 ml/min, and separation of the components was detected at the wavelength of 217 nm. Kinetic parameters were derived from three independent experiments in order to calculate the means and standard deviation (sd) for the K_m and k_{cat} values.

Data availability

The coordinates and the crystal structure factor of the silkworm JHAMT2, JHAMT2·SAH, and the JHAMT2·SAH·MF ternary complex have been deposited into the Protein Data Bank with the accession codes 7EBS, 7EBX, and 7EC0, respectively. All other data are available from the corresponding authors upon request.

Supporting information—This article contains supporting information.

Acknowledgments—We thank the staff at Shanghai Synchrotron Radiation Facility for the data collection. This work was supported by the National Natural Science Foundation of China (grant number 31970468 and 32030103), Natural Science Foundation of Chongqing, China (cstc2020jcyj-cxttX0001), the Venture and Innovation Support Program for Chongqing Overseas Returnees (cx2020100).

Author contributions—P. G., P. Z., and Q. X. conceptualization; Y. Z. data curation; Z. W. formal analysis; P. G. and Q. X. funding acquisition; P. G., Y. Z., and L. Z. investigation; Y. Z., L. Z., H. X., H. Z., and Y. J. methodology; H. Z. and P. Z. resources; H. X. and Y. J. software; P. Z. and Q. X. supervision; Y. Z., L. Z., H. X., Z. W., and D. M. validation; P. G. visualization; P. G. writing–original draft; D. M. and Q. X. writing–review and editing.

Conflict of interest—The authors declare that they have no conflicts of interest with the contents of this article.

Abbreviations—The abbreviations used are: FA, farnesoic acid; JH, Juvenile hormone; JHAMT, Juvenile hormone acid methyltransferase; MF, methyl farnesoate; SAH, S-adenosyl-L-homocysteine; SAM, S-adenosyl-L-methionine.

References

1. Goodman, W. G., and Granger, N. A. (2005) The juvenile hormones. *Compr. Mol. Insect Sci.* **3**, 319–408
2. Riddiford, L. M. (1994) Cellular and molecular actions of juvenile hormone I. General considerations and premetamorphic actions. *Adv. Insect Physiol.* **24**, 213–274
3. Li, Y., Hernandez-Martinez, S., Unnithan, G. C., Feyereisen, R., and Noriega, F. G. (2003) Activity of the corpora allata of adult female Aedes aegypti: Effects of mating and feeding. *Insect Biochem. Mol. Biol.* **33**, 1307–1315
4. Tobe, S. S., and Stay, B. (1985) Structure and regulation of the corpus allatum. *Adv. Insect Physiol.* **18**, 305–432
5. Wigglesworth, V. B. (1969) Chemical structure and juvenile hormone activity. *Nature* **221**, 190–191
6. Judy, K. J., Schooley, D. A., Dunham, L. L., Hall, M. S., Bergot, B. J., and Siddall, J. B. (1973) Isolation, structure, and absolute configuration of a new natural insect juvenile hormone from *Manduca sexta*. *Proc. Natl. Acad. Sci. U. S. A.* **70**, 1509–1513
7. Bergot, B. J., Jamieson, G. C., Ratcliff, M. A., and Schooley, D. A. (1980) JH zero: New naturally occurring insect juvenile hormone from developing embryos of the tobacco hornworm. *Science* **210**, 336–338
8. Harshman, L. G., Song, K. D., Casas, J., Schuurmans, A., Kuwano, E., Kachman, S. D., Riddiford, L. M., and Hammock, B. D. (2010) Bioassays of compounds with potential juvenoid activity on *Drosophila melanogaster*: Juvenile hormone III, bisepoxide juvenile hormone III and methyl farnesoates. *J. Insect Physiol.* **56**, 1465–1470
9. Jones, G., Jones, D., Li, X. B., Tang, L. F., Ye, L., Teal, P., Riddiford, L., Sandifer, C., Borovsky, D., and Martin, J. R. (2010) Activities of natural methyl farnesoids on pupariation and metamorphosis of *Drosophila melanogaster*. *J. Insect Physiol.* **56**, 1456–1464
10. Nagaraju, G. P. C. (2007) Is methyl farnesoate a crustacean hormone? *Aquaculture* **272**, 39–54
11. Kotaki, T., Shinada, T., Kaihara, K., Ohfune, Y., and Numata, H. (2009) Structure determination of a new juvenile hormone from a heteropteran insect. *Org. Lett.* **11**, 5234–5237
12. Li, S., Falabella, P., Kuriachan, I., Vinson, S. B., Borst, D. W., Malva, C., and Pennacchio, F. (2003) Juvenile hormone synthesis, metabolism, and resulting haemolymph titre in *Heliothis virescens* larvae parasitized by Toxoneuron nigriceps. *J. Insect Physiol.* **49**, 1021–1030
13. Belles, X., Martin, D., and Piulachs, M. D. (2005) The mevalonate pathway and the synthesis of juvenile hormone in insects. *Annu. Rev. Entomol.* **50**, 181–199
14. Lombard, J., and Moreira, D. (2011) Origins and early evolution of the mevalonate pathway of isoprenoid biosynthesis in the three domains of life. *Mol. Biol. Evol.* **28**, 87–99

15. Helvig, C., Koener, J. F., Unnithan, G. C., and Feyereisen, R. (2004) CYP15A1, the cytochrome P450 that catalyzes epoxidation of methyl farnesoate to juvenile hormone III in cockroach corpora allata. *Proc. Natl. Acad. Sci. U. S. A.* **101**, 4024–4029
16. Shinoda, T., and Itoyama, K. (2003) Juvenile hormone acid methyltransferase: A key regulatory enzyme for insect metamorphosis. *Proc. Natl. Acad. Sci. U. S. A.* **100**, 11986–11991
17. Niwa, R., Niimi, T., Honda, N., Yoshiyama, M., Itoyama, K., Kataoka, H., and Shinoda, T. (2008) Juvenile hormone acid O-methyltransferase in *Drosophila melanogaster*. *Insect Biochem. Mol. Biol.* **38**, 714–720
18. Wu, J. C., and Santi, D. V. (1987) Kinetic and catalytic mechanism of HhaI methyltransferase. *J. Biol. Chem.* **262**, 4778–4786
19. Li, W., Huang, Z. Y., Liu, F., Li, Z., Yan, L., Zhang, S., Chen, S., Zhong, B., and Su, S. (2013) Molecular cloning and characterization of juvenile hormone acid methyltransferase in the honey bee, *Apis mellifera*, and its differential expression during caste differentiation. *PLoS One* **8**, e68544
20. Dominguez, C. V., and Maestro, J. L. (2018) Expression of juvenile hormone acid O-methyltransferase and juvenile hormone synthesis in Blattella germanica. *Insect Sci.* **25**, 787–796
21. Mayoral, J. G., Nouzova, M., Yoshiyama, M., Shinoda, T., Hernandez-Martinez, S., Dolghih, E., Turjanski, A. G., Roitberg, A. E., Priestap, H., Perez, M., Mackenzie, L., Li, Y., and Noriega, F. G. (2009) Molecular and functional characterization of a juvenile hormone acid methyltransferase expressed in the corpora allata of mosquitoes. *Insect Biochem. Mol. Biol.* **39**, 31–37
22. Daimon, T., Uchibori, M., Nakao, H., Sezutsu, H., and Shinoda, T. (2015) Knockout silkworms reveal a dispensable role for juvenile hormones in holometabolous life cycle. *Proc. Natl. Acad. Sci. U. S. A.* **112**, E4226–E4235
23. Minakuchi, C., Namiki, T., Yoshiyama, M., and Shinoda, T. (2008) RNAi-mediated knockdown of juvenile hormone acid O-methyltransferase gene causes precocious metamorphosis in the red flour beetle *Tribolium castaneum*. *FEBS J.* **275**, 2919–2931
24. Cusson, M., Sen, S., and T, S. (2012) Chapter 3: Juvenile hormone biosynthetic enzymes as targets for insecticide discovery. In: Ishaaya, I., Palli, S., Horowitz, A., eds. *Advanced Technologies for Managing Insect Pests*, Springer, Dordrecht, The Netherlands: 31–55
25. Yin, Y., Qiu, Y. W., Huang, J., Tobe, S. S., Chen, S. S., and Kai, Z. P. (2020) Enzymes in the juvenile hormone biosynthetic pathway can be potential targets for pest control. *Pest Manag. Sci.* **76**, 1071–1077
26. Hiruma, K., and Kaneko, Y. (2013) Hormonal regulation of insect metamorphosis with special reference to juvenile hormone biosynthesis. *Curr. Top. Dev. Biol.* **103**, 73–100
27. Cheng, D., Meng, M., Peng, J., Qian, W., Kang, L., and Xia, Q. (2014) Genome-wide comparison of genes involved in the biosynthesis, metabolism, and signaling of juvenile hormone between silkworm and other insects. *Genet. Mol. Biol.* **37**, 444–459
28. Martin, J. L., and McMillan, F. M. (2002) SAM (dependent) I AM: The S-adenosylmethionine-dependent methyltransferase fold. *Curr. Opin. Struct. Biol.* **12**, 783–793
29. Holm, L. (2020) DALI and the persistence of protein shape. *Protein Sci.* **29**, 128–140
30. Suzuki, R., Fujimoto, Z., Shiotsuki, T., Tsuchiya, W., Momma, M., Tase, A., Miyazawa, M., and Yamazaki, T. (2011) Structural mechanism of JH delivery in hemolymph by JHBP of silkworm, *Bombyx mori*. *Sci. Rep.* **1**, 133
31. Lee, J. H., Bae, B., Kuemin, M., Circello, B. T., Metcalf, W. W., Nair, S. K., and van der Donk, W. A. (2010) Characterization and structure of DhpI, a phosphonate O-methyltransferase involved in dehydrophos biosynthesis. *Proc. Natl. Acad. Sci. U. S. A.* **107**, 17557–17562
32. Zhang, X., and Cheng, X. (2003) Structure of the predominant protein arginine methyltransferase PRMT1 and analysis of its binding to substrate peptides. *Structure* **11**, 509–520
33. Cusson, M., Sen, S. E., and Shinoda, T. (2013) Juvenile hormone biosynthetic enzymes as targets for insecticide discovery. In: Ishaaya, I., Palli, S. R., Horowitz, A. R., eds. *Advanced Technologies for Managing Insect Pests*, Springer Netherlands, Dordrecht: 31–55
34. Minor, W., Cymborowski, M., Otwinowski, Z., and Chruszcz, M. (2006) HKL-3000: The integration of data reduction and structure solution–from diffraction images to an initial model in minutes. *Acta Crystallogr. D Biol. Crystallogr.* **62**, 859–866
35. Vagin, A., and Teplyakov, A. (2010) Molecular replacement with MOLREP. *Acta Crystallogr. D Biol. Crystallogr.* **66**, 22–25
36. Potterton, L., Agirre, J., Ballard, C., Cowtan, K., Dodson, E., Evans, P. R., Jenkins, H. T., Keegan, R., Krissinel, E., Stevenson, K., Lebedev, A., McNicholas, S. J., Nicholls, R. A., Noble, M., Pannu, N. S., *et al.* (2018) CCP4i2: The new graphical user interface to the CCP4 program suite. *Acta Crystallogr. D Struct. Biol.* **74**, 68–84
37. Murshudov, G. N., Skubak, P., Lebedev, A. A., Pannu, N. S., Steiner, R. A., Nicholls, R. A., Winn, M. D., Long, F., and Vagin, A. A. (2011) REFMAC5 for the refinement of macromolecular crystal structures. *Acta Crystallogr. D Biol. Crystallogr.* **67**, 355–367
38. Emsley, P., and Cowtan, K. (2004) Coot: Model-building tools for molecular graphics. *Acta Crystallogr. D Biol. Crystallogr.* **60**, 2126–2132
39. Lovell, S. C., Davis, I. W., Arendall, W. B., 3rd, de Bakker, P. I., Word, J. M., Prisant, M. G., Richardson, J. S., and Richardson, D. C. (2003) Structure validation by calpha geometry: phi,psi and cbeta deviation. *Proteins* **50**, 437–450
40. DeLano, W. (2002) *The PyMOL Molecular Graphics System*, DeLano Scientific, San Carlos, CA
41. Corpet, F. (1988) Multiple sequence alignment with hierarchical clustering. *Nucleic Acids Res.* **16**, 10881–10890
42. Robert, X., and Gouet, P. (2014) Deciphering key features in protein structures with the new ENDscript server. *Nucleic Acids Res.* **42**, W320–W324
43. Laskowski, R. A., and Swindells, M. B. (2011) LigPlot+: Multiple ligand-protein interaction diagrams for drug discovery. *J. Chem. Inf. Model* **51**, 2778–2786